Layer-wise Profile Monitoring of Laser-based Additive Manufacturing

Seyyed Hadi Seifi[1], Wenmeng Tian[1], Haley Doude[2], Mark A. Tschopp[3], Linkan Bian[1,2]

[1]Industrial and Systems Engineering Department, Mississippi State University, MS 39762

[2]Center for Advanced Vehicular Systems, Mississippi State University, MS 39762

[3]Army Research Laboratory, Chicago, IL 60615

Abstract

Additive manufacturing (AM) is a novel fabrication technique capable of producing highly complex parts. Nevertheless, a major challenge is improving the quality of fabricated parts. While there are a number of ways of approaching this problem, developing data-driven methods that use AM process signatures to identify these part anomalies can be rapidly applied to improve overall part quality during build. The objective of this study is to build a new layer-wise process signature model to create the thermal-microstructure relationship. In this study, we derive novel key process signatures for each layer (from melt pool thermal images), which are reduced using multilinear principal component analysis (MPCA) and are directly correlated with layer-wise quality of the part. Using these key process signatures, a Gaussian SVM classifier model is trained to detect the existence of anomalies inside a layer. The proposed models are validated through a case study of real-world direct laser deposition experiment where the layer-wise quality of the part is predicted on the fly. The accuracy of the predictions is calculated using three measures (recall, precision, and f-score), showing reasonable success of the proposed methodology in predicting layer-wise quality. The ability to predict layer-wise quality enables process correction to eliminate anomalies and to ultimately improve the quality of the fabricated part.

1. Introduction

Additive manufacturing techniques fabricate parts with complex shapes in a layer-by-layer manner, significantly reducing material waste and enabling new design options that are not feasible with conventional manufacturing technologies [1]. However, a major barrier that prevents wider industrial adoption of AM is that the quality of manufactured parts does not meet the stringent requirements of industrial application due to the existence of defects (e.g. porosity, cracking, etc.). There is an urgent need to develop layer-based quality measures for deposited layers so that correction actions can be taken to improve part quality during the fabrication. Hence, establishing and quantifying the process-structure relationship of the metal additive manufacturing (AM) through new layer-based process signatures can provide great value towards tuning the part quality.

The challenges associated with the development of the efficient layer-wise process signature is two-fold. First, there is a lot of uncertainty in the underlying thermo-mechanical process of metal printing associated with the compositional and process parameters. Existing finite element methods (FEMs) have been used to model correlation between thermal history and microstructure properties. Temperature distribution and thermal behavior are the key properties in studying the thermomechanical process which affect the part stress, formation and hardness as well

as phase transformation during the AM process which have been studied thoroughly by Matsumoto et al., Kolossov et al., Crespo et al and Martukanitz et al. [2]–[5]. However, these approaches have several challenges that still need to be overcome: they are (1) dependent on part geometry, (2) time consuming, (3) non-robust to process uncertainty (deterministic nature), and (4) have high computational costs. Therefore, the current state of the art with FEMs cannot provide online predictions [6].

Second, advanced sensing technologies have been utilized to monitor the thermal history during fabrication. The resulting sensing data has high dimensionality and a low signal-to-noise ratio. Existing data-driven methods focus on robust statistical methods to detect anomalies from thermal images [10]–[12]. However, most of the existing works use local features for prediction purposes. Thus, they cannot be directly utilized to characterize the profile of an entire deposited layer. Hence, layer-wise modeling has attracted the attention of the additive manufacturing community. Layer-wise spatial porosity evolution has been previously modeled by Lie el al. based on X-ray computed tomography (XCT), which is a highly time consuming and expensive characterization technique [7]. Layer-wise defect monitoring based on advanced sensing systems has also been studied by Yao et al.[8].
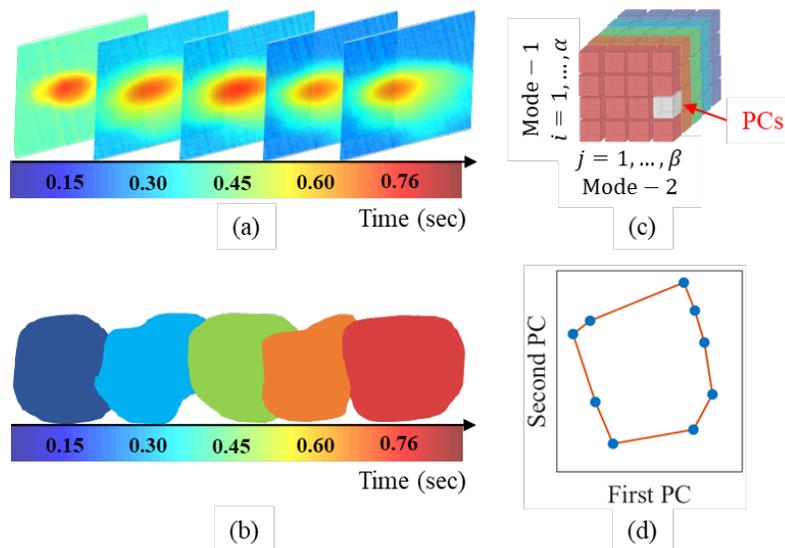

Figure 1: Illustration of the four main steps toward achieving the key signatures: (a) initial layer-based thermal images, (b) tensor structure of layer, (c) extracted principal components, and (d) layer-wise process signature.

In this work, we propose a data-driven methodology to extract thermal-based process signatures, which are directly correlated to the quality of the deposited layers. This represents a fundamental shift in the paradigm, from modeling and monitoring of individual melt pools to layer-based modeling. To address the issue of high dimensionality of thermal history images, we propose to develop a tensor-based modeling approach to characterize the highly dynamic thermal-physical AM process, captured by the pyrometer camera during the build (see Figure 1(a, b)). A central premise of the proposed methodology is that a uniform thermal history tends to lead to homogenous microstructure of the deposited layers, resulting in a more consistent part quality. To characterize the variability exhibited in the thermal history, multilinear PCA is utilized to extract the spatiotemporal variation of thermal images as a tensor (Figure 1 (c)). We propose a novel, layer-wise quality signature using a convex hull based on multilinear principal components of all

individual melt pools from the same layer (Figure 1 (d)). We examine the uniqueness and sensitivity properties of the layer-wise quality index and prove that it is the most proper index which characterizes the change of quality of the deposited layers. The proposed methodology is validated using a real-world direct laser deposition experiment in which the layer-wise thermal-based quality index predicts the distribution of porosity within the corresponding layers. This proposed new quality index provides the theoretical foundation for control/correction at laser based additive manufacturing (LBAM) process by accurately predicting the overall quality of deposited layers.

The remaining of the paper is organized as follows: Section 2 provides the mathematical background behind the proposed methodology, Section 3 introduces the case study used to validate the methodology and Section 4 is the conclusion.

2. <u>Methodology</u>

2.1.　　Data Description and Challenges

Thermal history is a term used to represent the thermal response (thermal cycling behavior) in manufactured parts as a function of time [9]. Thermal history is a signature of the build process and, thus, carries information about the microstructure of the part. Thermal history can be represented through images of melt pools captured by a pyrometer camera during the build. The melt pool is the region of superheated molten metal usually with a droplet shape that moves at a traverse speed [9]. Each image of melt pool includes location-based temperatures; therefore, each layer is a collection (video) of images. Dealing with layer-wise thermal history is challenging due to (1) high dimensionality of data, (2) corrupted and missing data, and (3) discrete sampling, where the number of melt pool samples are determined by the sampling frequency. Conventional approaches handle melt pool images one-by-one and provide predictions at the location of each individual melt pool. Therefore, these approaches do not deal with challenges concerning layer-wise modeling of thermal history.

In the following sections, we propose a method to reduce the dimensionality of images and through spatiotemporal variation between images, layer-wise key process signatures are extracted. Finally, the classification model is built upon key process signatures.

2.2.　　Data Transformation

Each melt pool is captured by the pyrometer camera as an image with a temperature reading at each pixel location within the field of views. Usually, the large size of these images (number of pixels) complicates processing without proper data reduction. Most important, the heat affected zone (HAZ) is usually condensed and carries the main features of the melt pool. Transforming the initial coordinate system and interpolating the temperature response surface can help to both emphasize the heat affected zone and reduce the data dimensionality. Converting the coordinate system from Cartesian to Spherical enables melt pools with different sizes, shapes, and locations to have identical support in the spherical domain [10]. Afterwards, incorporating a nonparametric surface interpolation (e.g., bi-harmonic model) allows data to be converted from discrete into continuous form. Having a continuous model in hand, a smaller grid of information can be extracted to effectively decrease the image size. Therefore, overall data dimensionality decreases

significantly. Considering the output of data transformation, each melt pool $\mathcal{M}_i$ is an image (tensor) with size $l \times k$. At this point, the next step is applying Multilinear Principal Component Analysis (MPCA)—a powerful tool for feature extraction and dimension reductions purposes.

2.3. Feature Extraction with MPCA

Multilinear Principal Component Analysis is a method developed [11] to extract features of high dimensional data expressed as tensors. One alternative approach is reshaping the melt pool data into large vectors (vectorization) and apply traditional Principal Component Analysis (PCA). However, vectorization causes computational and memory issues; moreover, vectorization breaks the natural correlation structure of original melt pool data [11]. MPCA is a dimensionality reduction algorithm that works directly on tensor objects instead of vectors.

A set of N tensor objects $\{\mathcal{M}_1, \mathcal{M}_2, \dots, \mathcal{M}_N\}$ is available for training. Each tensor object $\mathcal{M}_j \in \mathbb{R}^{I_1 \times I_2}$ accepts values from tensor space $\mathbb{R}^{I_1} \otimes \mathbb{R}^{I_2}$. The MPCA's goal is to perform a 2-mode transformation of the original tensor data into a low dimensional tensor subspace. The 2-dimensional melt pool data requires two projection matrices $\widetilde{U}^{(t)}$. Each projection matrix $\{\widetilde{U}^{(t)} \in \mathbb{R}^{I_t \times I_t'}, t = 1,2\}$ maps the tensor space $\mathbb{R}^{I_1} \otimes \mathbb{R}^{I_2}$ into a tensor subspace $\mathbb{R}^{I_1'} \otimes \mathbb{R}^{I_2'}$ where $I_t' < I_t$. The transformation equation is

$$\mathcal{M}_j' = \mathcal{M}_j \times_1 \widetilde{U}^{(1)^T} \times_2 \widetilde{U}^{(2)^T}, \qquad j = 1, \dots, N$$

where $\mathcal{M}_j' \in \mathbb{R}^{I_1' \times I_2'}$ captures most of the variation from original data.

2.4. Key Process Signatures of a Layer

Key process signatures carry the most valuable features to discriminate healthy layers from unhealthy ones. To improve the performance of MPCA, it is critical to train it based on the healthy melt pools and afterwards, applying the estimated projection matrices to all melt pools to extract their principal components (PCs). The reason behind this procedure is that the healthy melt pools carry the same temperature distribution and projecting any unhealthy melt pool (different temperature distribution) using the projection matrices of the healthy model will lead to a significant dissimilarity in either of the key process signatures of layers.

2.4.1. Primary Feature: Volume of the convex hull

The first key process signature is directly derived from the PCs resulted from MPCA. The main idea is to find a measure to capture the dispersion of the PCs of all melt pools within one layer. Being defected causes at least one melt pool to have a major difference in PCs compared to the healthy ones which leads to more scattered points (as shown in Figure 2). To capture the dispersion, one reasonable approach is building a convex hull using the multiple number of PCs for each melt pool. Although, other geometric shapes, such as sphere, can also be utilized to enclose the points, convex hull builds a unique free form shape around data points which is also highly sensitive to the change in data points. Two theorems stated below demonstrates the advantages of using the convex hull over the minimal bounding sphere.
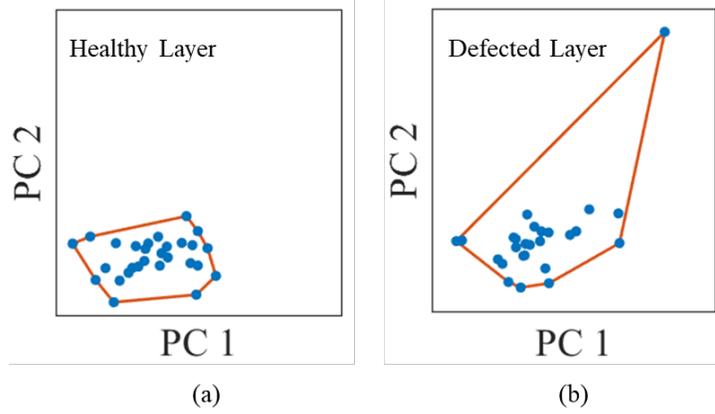
Figure 2: Illustration of the first layer-wise key signature. Examples of (a) a healthy layer and (b) an unhealthy layer.

Definition 1: Convex Hull

The convex hull of finite point set C is the intersection of all convex supersets containing C as $conv(C) = \{\sum_{i=1}^{n} \lambda_i c_i \,|\, c_i \in C, \lambda_i \geq 0, \sum_{i=1}^{n} \lambda_i = 1\}$ [12].

Definition 2: Minimal Bounding Sphere

The smallest bounding sphere $\omega(C)$ is the hypersphere with smallest radius which encloses a given point set C in its interior or on its boundary; i.e. $\|c_i - O\| \leq R, \forall\, i \in 1, \dots, n$, where O and R are the center and the radius of $\omega(C)$, respectively.

Theorem 1: Sensitivity

Adding a new point x^* to set C, $x \notin conv(C)$, the convex hull will definitely get enlarged. On the other hand, its smallest bounding sphere may not change.

Proof: If $\exists \lambda_i^* : x^* = \sum_{i=1}^{n} \lambda_i^* c_i$, $\lambda_i^* \geq 0, \sum_{i=1}^{n} \lambda_i^* = 1$, then $x^* \in conv(C)$ and $conv(C \cup \{x^*\}) = conv(C)$. Additionally, for the bounding sphere, $\|x^* - O\| = \|\sum_{i=1}^{n} \lambda_i^* (c_i - O)\| \leq \sum_{i=1}^{n} \lambda_i^* \|c_i - O\| \leq \sum_{i=1}^{n} \lambda_i^* R = R$, thus $\omega(C \cup \{x^*\}) = \omega(C)$.

If $\nexists \lambda_i^* : x^* = \sum_{i=1}^{n} \lambda_i^* c_i$, $\lambda_i^* \geq 0, and\ \sum_{i=1}^{n} \lambda_i^* = 1$, we need to add x^* to the basis of the convex combinations which updates the supersets and extends the convex hull to $conv(C \cup \{x^*\}) = \{\sum_{i=1}^{n} \lambda_i c_i + \lambda_{n+1} x^* | c_i \in C, \ \lambda_i \geq 0, \sum_{i=1}^{n+1} \lambda_i = 1\} \neq conv(C)$.

Moreover, regarding the bounding sphere, if $\|x^* - O\| \leq R$, $\omega(C \cup \{x^*\}) = \omega(C)$; and if $\|x^* - O\| > R$, the radius R needs to be enlarged to enclose x^*, i.e. $\omega(C \cup \{x^*\}) \neq \omega(C)$.

Theorem 2: Conditional Uniqueness

Each point set has its own unique convex hull provided a fixed set of extreme points.

Proof: Suppose we have one set of n points C. Assume that two different points $x_1^* \neq x_2^*$ are added separately to set C where

$$\nexists \lambda_i^* : x_1^* = \sum_{i=1}^{n} \lambda_i^* c_i, \lambda_i^* \geq 0, and\ \sum_{i=1}^{n} \lambda_i^* = 1$$
$$\nexists \lambda_i^* : x_2^* = \sum_{i=1}^{n} \lambda_i^* c_i, \lambda_i^* \geq 0, and\ \sum_{i=1}^{n} \lambda_i^* = 1$$

which means both points are exterior and according to Theorem 1, adding either of them to set C enlarges the convex hull into a new one where $conv(C \cup \{x_1^*\}) \neq conv(C \cup \{x_2^*\})$. On the other hand, if $\|x_1^* - O\| \leq R$ and $\|x_2^* - O\| \leq R$, the boundary sphere stays the same even though new

extreme points have been added to the set, i.e. $\omega(C \cup \{x_1^*\}) = \omega(C \cup \{x_2^*\})$. Overall, while convex hulls of two different sets are different, their corresponding minimal boundary spheres can be identical.

Volume of the convex hull decently measures the dispersion of the points. The more dispersion within data points, the more increase in volume of the convex hull. The algorithm on how to calculate the volume of a high-dimensional convex hull is provided in [13].

Although the convex hull is an effective measure for layer characteristics, the extracted PCs may not capture all the variation in data. Additionally, a valuable portion of information may get lost during projection from a higher dimension tensor to a lower dimension one. This is the reason why another signature feature should be introduced to account for the part not considered in primary feature.

Secondary Feature: Maximum Norm of Residuals

Each melt pool after projection loses a portion of data, whose amount differs from one melt pool to another. Backward projection of each melt pool using the projection matrices $\widetilde{U}^{(t)}$ will create a tensor which is of the same dimension as the initial input tensor to MPCA. Subtracting these two tensors generates the residual tensor. Backward projection is

$$\mathcal{M}_j'' = \mathcal{M}'_j \times_1 \widetilde{U}^{(1)} \times_2 \widetilde{U}^{(2)}, \; j = 1, \dots, N$$

where $\mathcal{M}_j''$ accepts value from tensor space $\mathbb{R}^{I_1} \otimes \mathbb{R}^{I_2}$, same as its initial tensor $\mathcal{M}_j$. Therefore, the residual tensor is $\mathcal{R} = \mathcal{M}_j - \mathcal{M}_j''$. One way to represent this residual tensor is through Euclidian norm, sometimes called the L^2 norm.
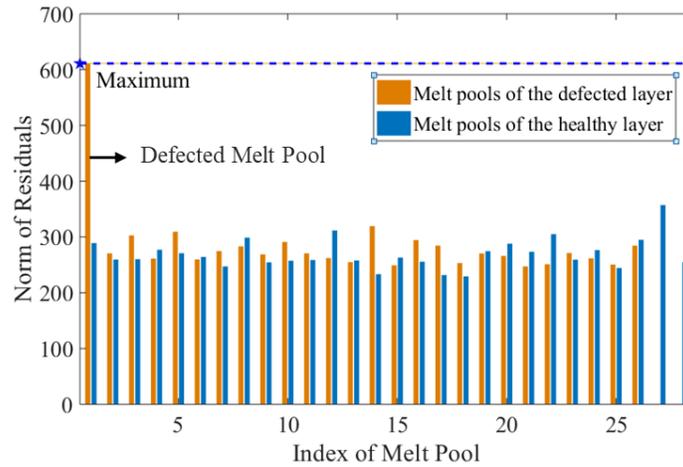

Figure 3: Demonstration of norm of residuals for melt pools of two layers. Orange bars are the norms for melt pools of the unhealthy layer where blue bars are for healthy layer. Other than first unhealthy melt pool, all the healthy melt pools have similar L2-norm residual.

Since MPCA is trained using healthy melt pools, it is expected that projecting defected melt pools results in bigger residuals than healthy ones. Choosing the maximum norm of residuals inside a layer (maximum between melt pools) is the most effective way of capturing anomalies. If there exists at least one unhealthy melt pool inside a layer, it causes the maximum norm of residuals to

increase noticeably (as shown in Figure 3). This is a similar idea with the group control chart in statistical quality control [14].

2.5.   Classification: Correlating Layer Signatures to Structural Quality

After defining the signature features, the convex hull volume, and the norm of residuals, the classification model can be trained. The goal of the classifier is to draw a boundary between healthy layers and defected layers. Moreover, it should be able to predict the labels of newly observed layers. As mentioned before, if one layer contains at least one porosity, it is labeled as unhealthy (as shown in Figure 4). The classifier's input is one vector of response labels (0 if healthy, 1 if unhealthy) and a matrix of two predictors: the convex hull volume and the maximum norm of residuals.

Choosing a classification technique is a critical step. The classifier should be powerful enough to discriminate the healthy layers from unhealthy ones and additionally, it should not over-fit the data with unnecessary complications. Support Vector Machine (SVM) is a powerful classification technique with a variety of kernel functions. Gaussian SVMs have the most flexibility among SVM classifiers. Fine Gaussian SVM makes finely detailed distinctions between classes (at the cost of overfitting in some cases). Medium Gaussian SVM has lower flexibility than Fine Gaussian and prevents overfitting issue. Medium Gaussian SVM is the suitable choice of classification in this study.
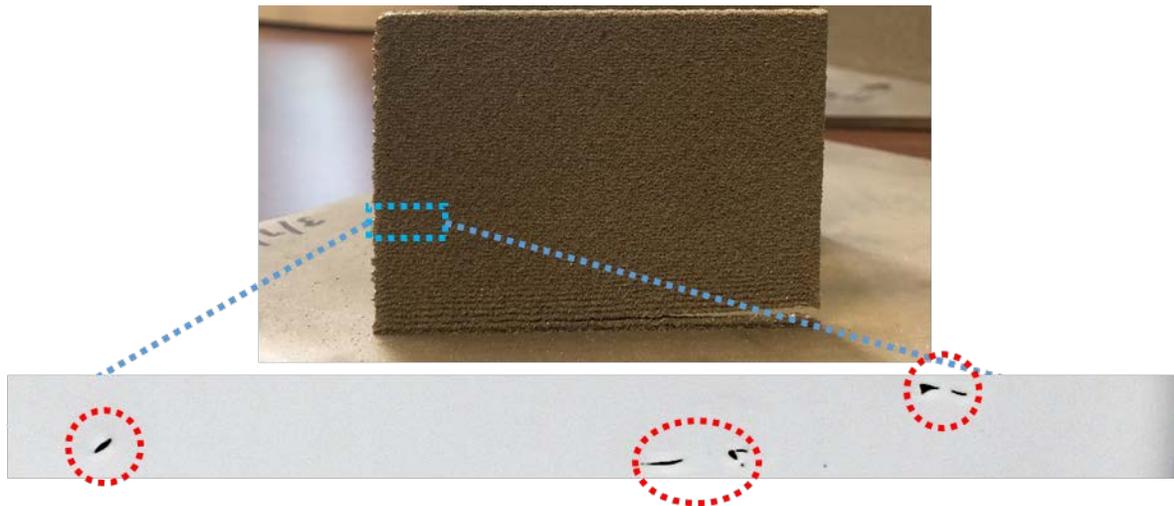

Figure 4: The illustration of part of unhealthy layer which includes pores.

3. Case Study

The performance of the proposed methodology is examined using a direct laser deposition process which fabricates a thin wall Ti-6AL-4V. During the build of this thin wall, a pyrometer camera has captured the thermal images of the melt pools at different locations of the thin wall. Afterwards, X-ray scans are used to characterize the layer-wise porosity structure inside the build.

The aforementioned thin wall includes 60 layers where each layer contain several melt pools in temporal order. Out of the 60 layers, 26 layers include at least one pore. These 60 layers

of data are divided into two sets, first part of data is used to train the model and second part is used to test the performance of the classifier. Before dividing data into training set and testing set, all thermal images are transformed into spherical coordinates and interpolated with a bi-harmonic model. Interpolation model is used to extract a lower dimensional grid of data. In thin wall data, each image with size 130×130 is transformed into a new grid with size 27×32.

After data transformation, key signature features are extracted and classification model is trained. Two types of cross validation techniques are discussed to analyze the performance of the proposed method.

The number of PCs chosen to form a convex hull for each layer affects the output of prediction. Sensitivity analysis is a reasonable approach for determining which number of PCs ends up with better classification and F-score. Figure 5 shows the calculated f-scores for dimensions (number of PCs) varying from 2 to 11. According to Figure 5, choosing 7 PCs (7 dimensional convex hull) leads to a better classification.
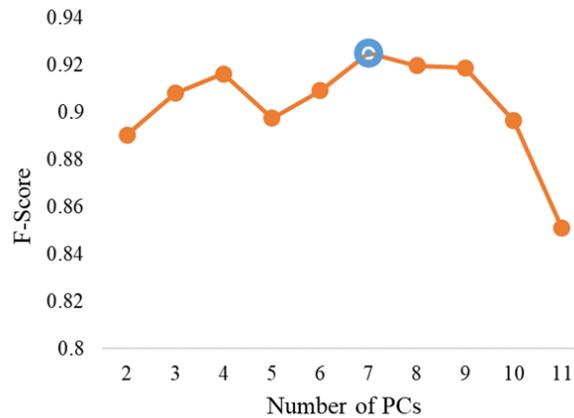

Figure 5: Effect of number of PCs in F-Score of classification

3.1.   Leave-one-out Cross Validation

Leave-one-out is an *N*-fold cross validation where *N* represents the number of samples. The confusion matrix after applying the model for 60 layers is shown in Table 1.

Out of 60 layers, 4 layers are misclassified where one is healthy and three others are unhealthy. The accuracy of model can be defined with three measures namely precision, recall and F-score. These measure can be calculated using below formulas.

$$\text{Recall} = \frac{\text{True Positive}}{\text{True Positive} + \text{False Negative}}$$

$$\text{Precision} = \frac{\text{True Positive}}{\text{True Positive} + \text{False Positive}}$$

F-score is the harmonic mean of precision and recall.

$$F - Score = 2 \times \frac{Precision \times Recall}{Precision + Recall}$$

Table 1: Confusion Matrix for the Leave-one-out Cross Validation

		Predicted	
		Healthy	Unhealthy
Actual	Healthy	33 (97%)	1 (3%)
	Unhealthy	3 (11.5%)	23 (88.5%)

For leave-one-out cross validation, the recall is equal to 0.88 and precision is equal to 0.96. The classification model accuracy is reasonably high (F-score is 0.92). To investigate the misclassified layers, first it is necessary to classify all of the layers. According to Figure 6, three of the unhealthy layers are misclassified which are the same layers as the ones misclassified in leave-one-out cross validation. Three of the unhealthy layers are behaving as healthy layers and this may be due to the missing data points within layers during sampling with the pyrometer camera. Removing these misclassified layers from the training set causes the classifier to correctly predict the one misclassified healthy layer, increasing precision and F-score to 1.00 and 0.94, respectively.
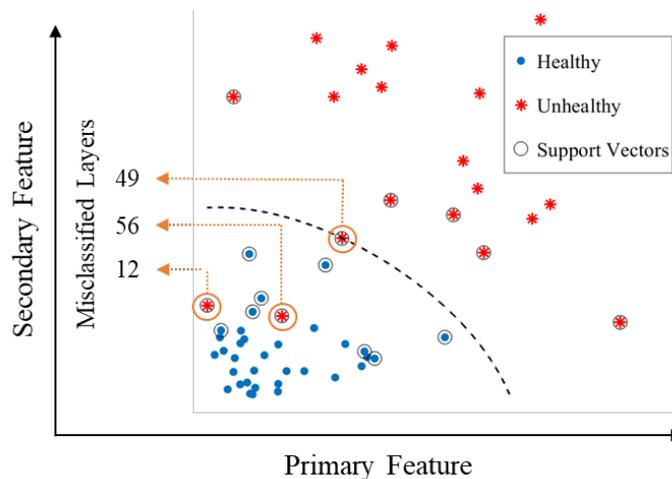

Figure 6: Full classification of all 60 layers

3.2. Monte-Carlo Cross Validation

Repeated random sub-sampling validation, also known as Monte-Carlo cross validation [15], randomly splits dataset into training and testing (validation) sets. Out of 60 layers, 50 layers are assigned randomly to training set which are later used to train the classifier and remaining 10 layers are chosen to test the classifier.

This random selection is performed 1000 times and all the three measures are calculated for each iteration. In each iteration, misclassified layers are removed from training set until all the layers are classified correctly. The mean and standard deviation (SD) value of the recall, precision and f-score are shown in Table 2.

Table 2: Illustration of random cross validation output in terms of three measures

	Recall	Precision	F-Score
Mean	0.8774	0.9857	0.9195
SD	0.1509	0.0647	0.0979

One output of one iteration is illustrated in Figure 7 where there exist 7 healthy and 3 unhealthy layers in the testing set. The classifier is trained using 50 random layers and misclassified layers are removed to the point where there is no misclassified layer. Having the classifier model in hand, a prediction is made for the layers in the testing set. 9 out of 10 layers are classified correctly and only one unhealthy layer is misclassified. The classification model uses medium Gaussian to classify the layers, which is shown with black dotted line in Figure 7. The bottom-left region of the line is classified as healthy.
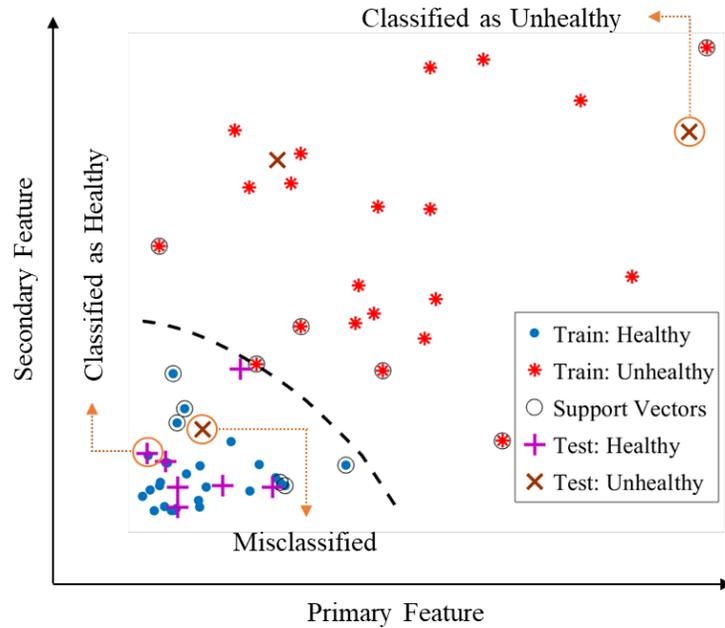

Figure 7: Illustration of one iteration of Monte Carlo cross validation

4. Conclusion

The main challenge in additive manufacturing process is its lack of repeatability which leads to quality issues such as internal porosity in the build. Extensive studies have been focused to address the quality issue, including data-driven methods that provide a local prediction based on single melt pools. The major contributions of this study include

1. A data-driven dimension reduction technique is used to decompose melt pool images based on MPCA;
2. Two novel layer-wise process signatures are proposed based on thermal history of the entire layer;

3. The SVM classifier is used for real-time layer-wise quality prediction

This proposed model will provide the foundation for online control/correction actions for LBAM processes by accurately predicting the layer-wise quality in real time.

5. <u>Acknowledgement</u>

6. <u>References</u>

[1]   M. Grasso and B. M. Colosimo, "Process defects and *in situ* monitoring methods in metal powder bed fusion: a review," *Meas. Sci. Technol.*, vol. 28, no. 4, p. 44005, Apr. 2017.

[2]   M. Matsumoto, M. Shiomi, K. Osakada, and F. Abe, "Finite element analysis of single layer forming on metallic powder bed in rapid prototyping by selective laser processing," *Int. J. Mach. Tools Manuf.*, vol. 42, no. 1, pp. 61–67, 2002.

[3]   S. Kolossov, E. Boillat, R. Glardon, P. Fischer, and M. Locher, "3D FE simulation for temperature evolution in the selective laser sintering process," *Int. J. Mach. Tools Manuf.*, vol. 44, no. 2–3, pp. 117–123, 2004.

[4]   A. Crespo, A. Deus, and R. Vilar, "FINITE ELEMENT ANALYSIS OF LASER POWDER DEPOSITION OF TITANIUM," 2005.

[5]   R. Martukanitz *et al.*, "Toward an integrated computational system for describing the additive manufacturing process for metallic materials," *Addit. Manuf.*, vol. 1, pp. 52–63, 2014.

[6]   M. Khanzadeh, S. Chowdhury, M. Marufuzzaman, and M. A. Tschopp, "Porosity prediction: Supervised-learning of thermal history for direct laser deposition Data analytics and statistical learning in Additive Manufacturing View project Deformation in HCP materials View project," *Artic. J. Manuf. Syst.*, 2018.

[7]   J. Liu *et al.*, "Layer-Wise Spatial Modeling of Porosity in Additive Manufacturing Real-time process monitoring for advanced manufacturing View project Sensing and Data Analytics for Additive Manufacturing View project Layer-wise Spatial Modeling of Porosity in Additive M," vol. 10, no. May, 2018.

[8]   B. Yao, F. Imani, and H. Yang, "Markov Decision Process for Image-guided Additive Manufacturing," *IEEE Robot. Autom. Lett.*, pp. 1–1, 2018.

[9]   S. M. Thompson, L. Bian, N. Shamsaei, and A. Yadollahi, "An overview of Direct Laser Deposition for additive manufacturing; Part I: Transport phenomena, modeling and diagnostics," *Addit. Manuf.*, vol. 8, pp. 36–62, 2015.

[10]   M. Khanzadeh, S. Chowdhury, M. A. Tschopp, H. R. Doude, M. Marufuzzaman, and L. Bian, "In-situ monitoring of melt pool images for porosity prediction in directed energy deposition processes," *IISE Trans.*, vol. 5854, pp. 1–19, 2018.

[11]   H. Lu, K. N. Plataniotis, and A. N. Venetsanopoulos, "MPCA: Multilinear principal component analysis of tensor objects," *IEEE Trans. Neural Networks*, vol. 19, no. 1, pp. 18–39, 2008.

[12]   J. Matoušek, *Lectures on discrete geometry*, vol. 212. Springer New York, 2002.

[13]   C. B. Barber, D. P. Dobkin, and H. Huhdanpaa, "The quickhull algorithm for convex hulls," *ACM Trans. Math. Softw.*, vol. 22, no. 4, pp. 469–483, Dec. 1996.

[14]   L. S. Nelson, "Control Chart for Multiple Stream Processes," *J. Qual. Technol.*, vol. 18, no. 4, pp. 255–256, Oct. 1986.

[15]   W. Dubitzky, M. Granzow, and D. P. Berrar, *Fundamentals of data mining in genomics and proteomics*. Springer Science & Business Media, 2007.